CRYSTAL GROWTH & DESIGN

pubs.acs.org/crystal

Article

Double Trouble: A Peculiar Case of Solid Solution Cocrystals Involving Two Chiral Compounds

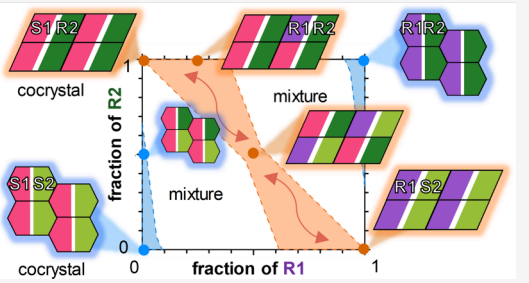
Sarita Songsermsawad, Oleksii Shemchuk, Koen Robeyns, Fuli Zhou, Adrian E. Flood,* and Tom Leyssens*

Cite This: *Cryst. Growth Des.* 2024, 24, 2977−2984

Read Online

ACCESS | Metrics & More | Article Recommendations | Supporting Information

ABSTRACT: Cocrystals have been widely studied in the context of chiral resolution. Enantiospecific and diastereomeric cocrystal resolution processes, as well as preferential resolution based on cocrystallization, are becoming more and more common. The formation of solid solutions is a rare phenomenon (less than 1% of compounds), with solid solutions between cocrystallization of two racemic compounds rarely described. In this contribution, we study such a case between two chiral compounds, 2-(2-Oxopyrrolidin-1-yl)butanamide (**1**) and methylsuccinic acid (**2**). Both diastereomers *S*-**1**:*S*-**2** and *S*-**1**:*R*-**2** form double-sided solid solutions, which are solid solutions where the enantiomers of either **1**, **2**, or both **1** and **2** can be partially replaced by their counterparts. Solid solution formation was proven by the observed disorder in the crystal structures. The limits of each solid solution are determined through a solid-state stability diagram. A double-sided solid solution based on cocrystallization offers potential as enantiomeric excess of both components can be varied with a given degree of freedom, without changing the nature of the solid phase present.



Downloaded via UNIV CATHOLIQUE DE LOUVAIN on June 10, 2024 at 13:15:39 (UTC).
See https://pubs.acs.org/sharingguidelines for options on how to legitimately share published articles.

1. INTRODUCTION

The number of studies related to cocrystals has strongly increased in the past 20 years, especially those involving pharmaceutical compounds. Cocrystals are alternative solid forms[1] used for modifying the physical properties of active pharmaceutical ingredients (APIs) without changing pharmacological effects.[2−4] There has been significant debate related to the definition of a cocrystal.[5] In this contribution, we consider a cocrystal to be a structurally homogeneous crystalline material consisting of two or more neutral molecular species that are solid under ambient conditions. The molecules comprising the cocrystal are present in a defined stoichiometric ratio, and connected through weak interactions (other than covalent and ionic bonds).[6]

Solid solutions are crystalline materials, in which components are miscible in a single phase. They can offer key advantages as in principle their properties can be altered by freely adjusting the proportion of the constituent components.[7] Both cocrystal and solid solution formation are valid crystal engineering techniques to enhance physicochemical properties, with recent studies[8−10] showing how both concepts can be used to fine-tune target properties. Solid solution cocrystals involving chiral compounds often occur due to a change in the enantiomeric ratio of the chiral compound.[11] If the counter enantiomers are partially miscible, the term partial solid solution[12−15] is used, whereas a complete solid solution is obtained if substitution occurs over the whole range of enantiomeric ratios.[16−19] Cappuccino et al. investigated such systems looking into the cocrystallization of praziquantel with malic acid and tartaric acid.[10] In their study racemic praziquantel and an equivalent amount of malic acid and/or tartaric acid formed complete solid-solution cocrystals with a freely varying enantiomeric ratio of tartaric acid or malic acid. Furthermore, these systems allowed for an increase in solubility compared to the pure drug.

Cocrystallization is not only used for improving physical properties but has also seen an increasing use as a tool for chiral resolution.[20] Chiral resolution by crystallization is an important path toward enantiopure drugs which often demonstrate higher clinical efficacy compared to racemic drugs, as well as being safer or having less side-effects than their racemic counterparts.[21] Various techniques have been developed for separation of racemic compounds by formation of cocrystals.

A first technique focuses on resolution by cocrystallization with an achiral compound aiming to form conglomerate cocrystals which can then be separated by preferential crystallization.[22−26] Care has to be taken, as for some systems solid solutions are formed instead of conglomerate cocrys-

Received: January 17, 2024
Revised: March 1, 2024
Accepted: March 1, 2024
Published: March 12, 2024



ACS Publications

© 2024 American Chemical Society

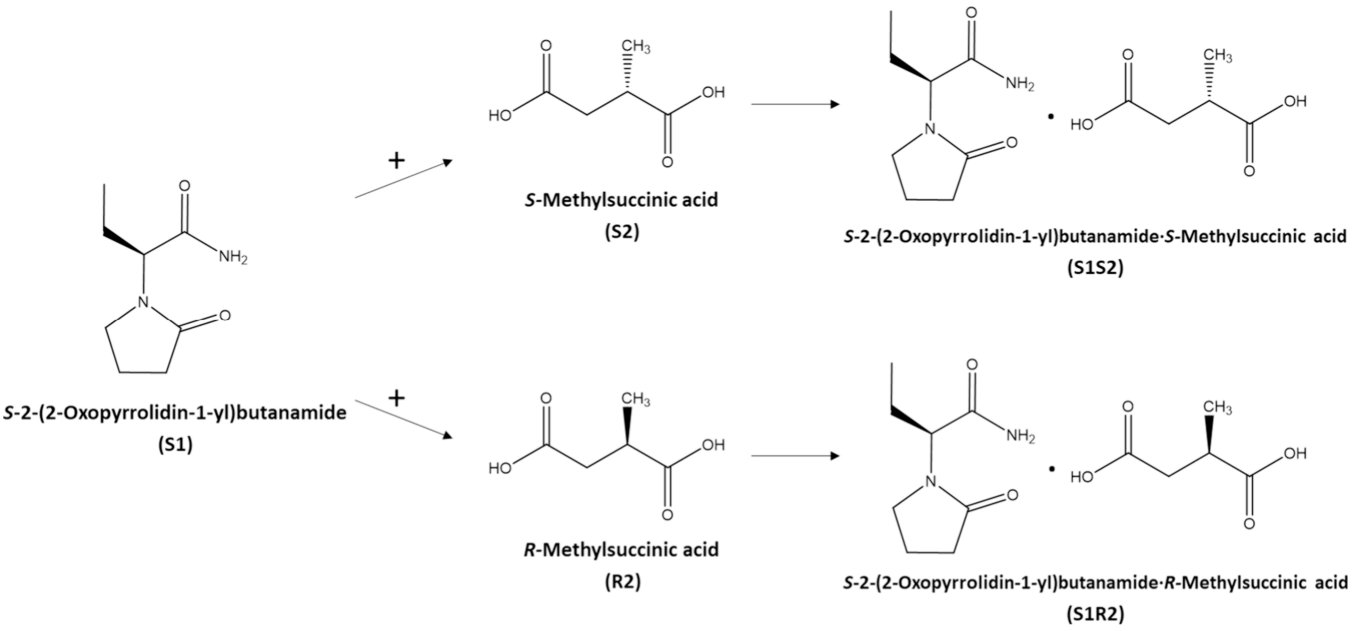


Figure 1. Schematic diagram showing the diastereomeric cocrystal pair formed between **1** and **2**.

tals.[13,16−19] In a second approach an enantiopure coformer can be combined with a racemate of the target compound, with the goal of developing either an enantiospecific or diastereomeric cocrystal resolution process.[27] Enantiospecific cocrystallization occurs when a chiral coformer interacts with only one of the enantiomers of the target compound whereas diastereomeric cocrystallization occurs when a pair of diastereomeric cocrystals can be formed.[28−30] In a third and final approach, a racemic resolution agent can be used. In a recent contribution, we successfully used *RS*-mandelic acid to resolve *RS*-etiracetam by forming a conglomerate comprising two chiral compounds.[31] Both racemic compounds were resolved simultaneously through a preferential crystallization process. We showed that formation of such a conglomerate is a rather rare feature, with a higher likelihood of forming "racemic−racemic" cocrystals.[32]

In this contribution, we build upon this work[32] showing that the combination of two racemic compounds can lead to further peculiar cases. Specifically, we encountered a double solid solution cocrystal, in which a given enantiomer of either of the composing chiral constituents can be freely replaced by its counter enantiomer. This occurs for the cocrystal between 2-(2-oxopyrrolidin-1-yl)butanamide (**1**) and methylsuccinic acid (**2**). Both **1** and **2** are known to crystallize as racemic compounds.[33−35] *RS*-2-(2-Oxopyrrolidin-1-yl)butanamide (etiracetam, RS1) is a racemic precursor to the enantiopure *S*- enantiomer, being the active ingredient of Keppra. The *S*-enantiomer (S1), known as Levetiracetam is more active than the *R*-enantiomer (R1) and used to treat epilepsy.[36] **2** is used as starting material in the pharmaceutical industry.[37] It was shown previously that grinding enantiopure combinations of these two compounds resulted in cocrystal formation as shown in Figure 1.[30] Mixing S1 with *S*-methylsuccinic acid (S2) and *R*-methylsuccinic acid (R2) leads to a diastereomeric cocrystal pair S1S2 and S1R2.

In this study, we focus on the four-component system comprised of an equimolar mixture of **1** and **2** in various combinations of both enantiomers. The stereochemical relationship between the four possible combinations is shown in Figure 2. Interestingly, the two cocrystal phases (S1R2 and S1S2) showed double-sided partial solid solutions

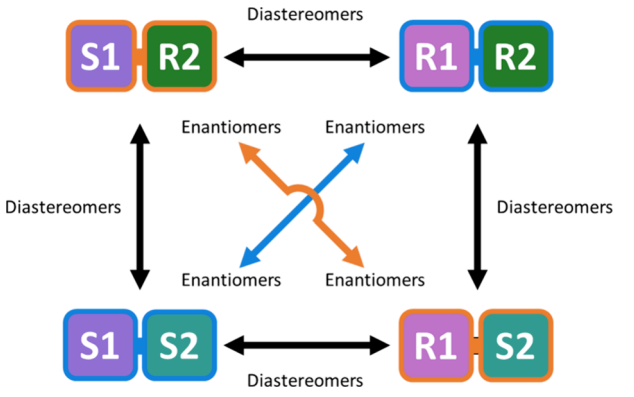


Figure 2. Schematic diagram showing the diastereomeric and enantiomeric relationship between the cocrystals.

allowing substitution of enantiomers of either of both compounds. Moreover, the S1R2 phase forms a complete solid solution by substitution with the counter-enantiomer R1S2. To the best of our knowledge this is the first report of the formation of a double solid solution.

2. EXPERIMENTAL SECTION

2.1. Materials. *S*-2-(2-Oxopyrrolidin-1-yl)butanamide (S1) was purchased from Xiamen Top Health Biochem Tech. Co., Ltd. *RS*-Methylsuccinic acid (RS2) was purchased from Sigma-Aldrich. *R*-Methylsuccinic acid (R2) was purchased from Tokyo Chemical Industry Co. (TCI). *S*-Methylsuccinic acid (S2) was purchased from Apollo Scientific. Methanol (99.8%), toluene (99.5%), dichloromethane (99.5%), and ethyl acetate (99.5%) were purchased from VWR International. These chemicals and solvents were used as received without further purification. *RS*-2-(2-Oxopyrrolidin-1-yl)-butanamide (RS1) was racemized from S1 by adding 10 g of S1 and a catalytic amount (0.05 equiv) of sodium methoxide to 10 mL of methanol. The solution was kept at reflux under continuous stirring for 24 h and then cooled to room temperature. The compound

https://doi.org/10.1021/acs.cgd.4c00074
Cryst. Growth Des. 2024, 24, 2977−2984

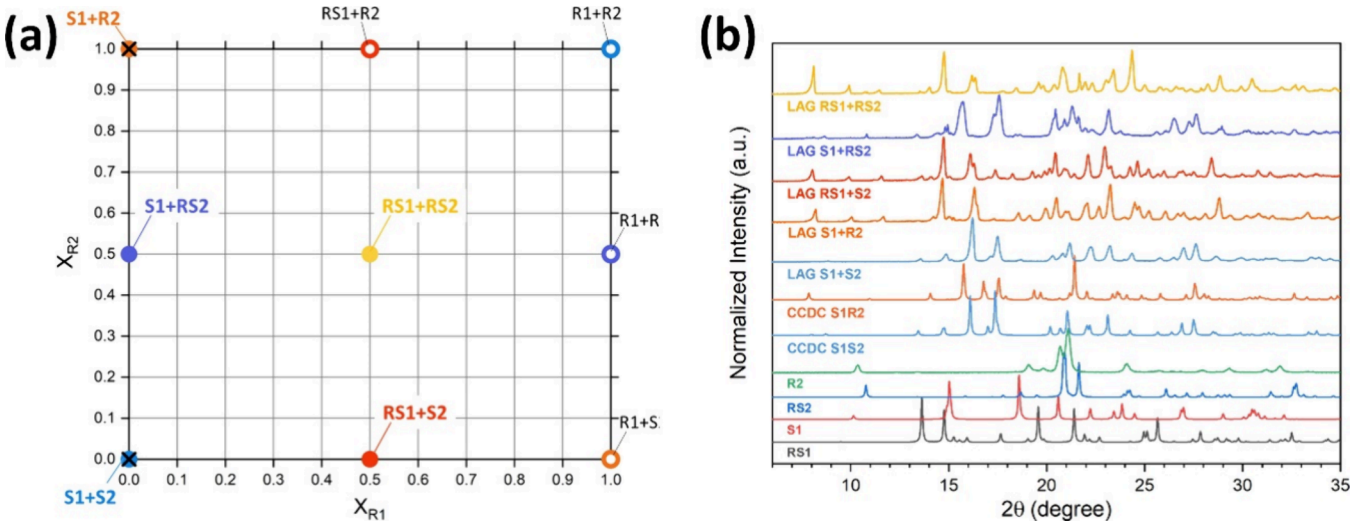


Figure 3. (a) Schematic diagram representing the screening experiments. The grinding combinations that were performed in previous work are represented by crosses and those new to this study by circles. Hollow circles represent mirror-image combinations. (b) XRPD patterns of grinding experiments between **1** and **2**, and comparison with the patterns of the reactants (RS1, S1, RS2, and R2) and the simulated patterns of S1S2 (CSD-REFCODE ROQLEQ) and S1R2 (CSD-REFCODE YAMQAH).

crystallizes spontaneously. After filtration, the compound was washed twice with methanol. The recovered compound was then used in the cocrystallization experiments described below.

2.2. Liquid-Assisted Grinding (LAG). LAG was performed in a RETSCH mixer mill MM400 using a frequency of 30 Hz for 1.5 h. The LAG experiments of five combinations (S1 + R2, S1 + S2, RS1 + R2, S1 + RS2, and RS1 + RS2) were done in 2 mL plastic milling jars containing three 3 mm stainless steel balls. For further grinding experiments, a bigger jar and bigger balls were used to avoid nonhomogeneous products; in these experiments a 10 mL zirconium milling jar containing two 5 mm zirconium balls were used. At the beginning of each test, 5 μL of methanol was added to 150 mg of an equimolar mixture of **1** and **2** before grinding. The ground samples were dried for 24 h and were then analyzed by X-ray powder diffraction (XRPD).

2.3. Crystal Structure Determination. The first attempt of crystallization of S1 + R2, RS1 + R2, S1 + RS2, and RS1 + RS2 combinations were done in methanol, ethyl acetate, dichloromethane, and methanol, respectively, by evaporative crystallization. Compounds **1** and **2** were added in amounts close to their solubilities in the respective solvent and the solvents were then evaporated until crystallization occurred. Details on crystallization conditions of each crystal are provided in Table S1. Single crystals were harvested from the solutions for structure determination. Diffraction data were collected on a MAR345 image plate using MoKα radiation generated by an Incoatec IμS microfocus source (Montel Mirrors). Data reduction was carried out using the CrysAlis^{PRO} software package.[38] The resolution and refinement by full-matrix least-squares were carried out using respectively SHELXT[39] and SHELX-2018/3.[40] Non-hydrogen atoms were refined anisotropically; H atoms were added in calculated positions and allowed to ride on the parent atoms, with isotropic displacement factors set to 1.2 Ueq of the parent atoms (Uiso(H) = 1.5 Ueq(C) for methyl and OH hydrogens). For the structures showing disorder (solid solutions), the disorder presents itself as R/S disorder where both enantiomers are superposed onto each other, while maintaining the same hydrogen bond interactions. Isotropic and rigid bond restraints were set up for all disordered atoms and the minor component was geometrically refined to be similar to the main component and occupancies were freely refined.

The other crystallizations were performed in toluene as the solvent screening showed that cocrystals between **1** and **2** behaved congruently in this solvent and the solubilities are relatively low compared to other solvents. All crystallization experiments were performed by slow cooling. Each sample contained 160 mg of an equimolar mixture of **1** and **2** (90 mg of **1** and 70 mg of **2**). The enantiomeric ratio of **1** and **2** was varied in each experiment combining racemic and enantiopure compounds, but the overall mass of **1** or **2** was not changed. Details on crystallization conditions of each crystal are provided in Table S1. To the powder was added 2 mL of toluene and the suspension was heated to 90 °C. Solvent was added until all solid was dissolved. The solutions were then slowly cooled to room temperature (20 °C) and left until crystallization occurred.

2.4. Solid-State Stability Diagram. The solid-state stability diagram shows the stable phase with respect to the enantiomeric compositions of cocrystal constituents. The diagram is limited to the solid phases and does not include any solvent, as this goes beyond the scope of this work. The diagram was constructed to visualize the miscibility limits of the partial solid solution cocrystals between **1** and **2**. For a diastereomeric cocrystal system, the limiting composition of each partial solid solution can be found by analyzing single crystals obtained from zones where both diastereomers form, as illustrated in the ternary diagram in Figure S1.[41,42] To minimize complexity, an equimolar ratio between **1** and **2** was used for all experiments and only the enantiomeric excess (*ee*) of both **1** and/or **2** was varied. Initially, LAG was used to obtain a rough estimation of the solid-state miscibility limit. At the extremes, only one solid phase was identified. Gradually changing the *ee* of one component, the same phase is obtained up to a given limit, after which two phases are observed. Increasing the *ee* further leads to the second limit for which once more only a single phase is identified. The exact *ee* for both limits was then confirmed by cooling crystallization experiments. When crystals of both diastereomeric phases were present in the same sample produced from a cooling experiment, crystals of each phase (showing a different crystal morphology) were harvested and analyzed by SC-XRD to calculate the composition. These compositions represent the true miscibility limit of each diastereomer. After mounting single crystals from the sample, the remaining bulk solid was filtered, dried, and analyzed by XRPD to confirm that both phases can indeed be observed in the bulk sample. This method successfully allowed identification of the phase boundary by varying the *ee* of one compound and using enantiopure material of the second compound. Experiments where both scalemic mixtures of **1** and **2** were used were only performed by LAG due to the difficulty in obtaining good crystals under these compositions. The mechanochemical product was assumed to be the thermodynamically stable solid. The limiting points from grinding were indicated as ranges to emphasize the inherent imprecision of these.

https://doi.org/10.1021/acs.cgd.4c00074
Cryst. Growth Des. 2024, 24, 2977−2984

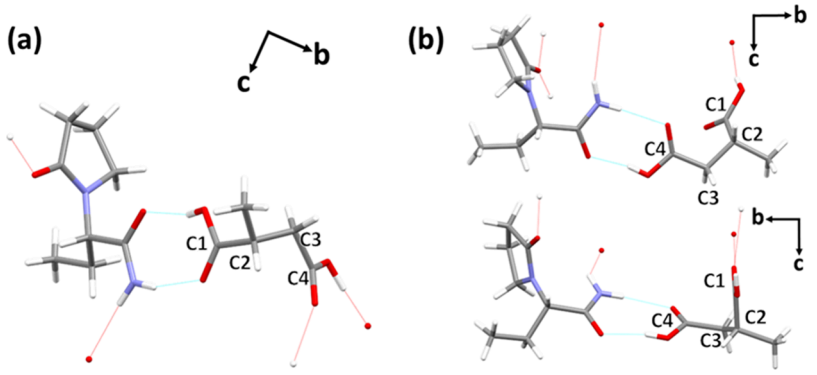


Figure 4. 3D representation of synthons of S1R2 (a) Form I and (b) Form II.

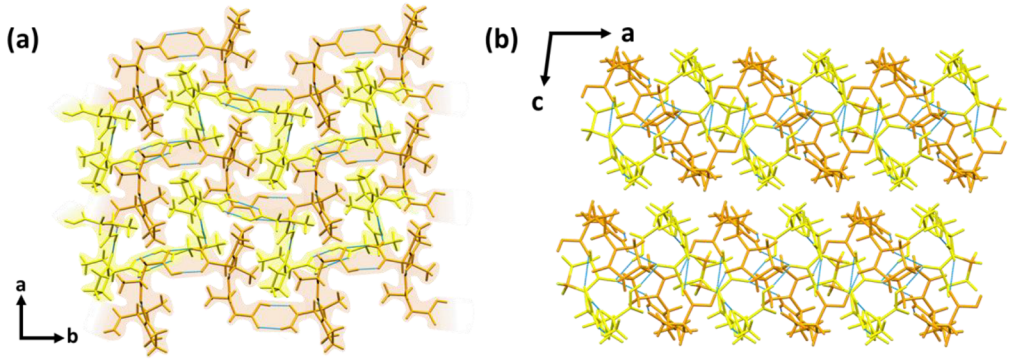


Figure 5. Crystal packing of S1R2 Form II with each color representing a conformation/spiral (a) along *ab* plane and (b) along *ac* plane.

2.5. X-ray Powder Diffraction (XRPD). XRPD patterns of the samples were measured on a Bruker D8 Advance powder X-ray diffractometer equipped with a Cu−Kα X-ray source (λ = 1.5406 Å) operating at 40 kV and 30 mA. The data were collected within 2θ values from 6 to 35° at a scan rate of 12°/min.

3. RESULTS AND DISCUSSION

In our previous work, the diastereomeric cocrystals S1S2 and S1R2 were identified by liquid-assisted grinding (LAG).[30] Besides repeating these two combinations, the remaining combinations between **1** and **2**, RS1 + S2, S1 + RS2, and RS1 + RS2, were also investigated.[43,44] Combinations R1 + R2, R1 + S2, RS1 + R2, and R1 + RS2 can be safely ignored as they are mirrored by one of the performed experiments (Figure 3a, hollow circles). The grinding combinations performed in this study are visualized in Figure 3a. The *x*-axis represents the mole fraction of *R*- for compound **1** (X_{R1}), while the *y*-axis shows the mole fraction of *R*- for compound **2** (X_{R2}). The powders from each grinding experiment were analyzed by XRPD, with the patterns shown in Figure 3b.

Results show that LAG products of S1 + S2 and S1 + R2 form new solid phases that differ from both reactants. The diastereomeric cocrystal pair S1S2 and S1R2 was already identified previously.[30] When comparing the simulated patterns from literature with the ones found here, the same phase is obtained for S1S2 (CSD-REFCODE ROQLEQ), but the experimental pattern of S1R2 does not match the phase identified in the earlier work (S1R2 with CSD-REFCODE YAMQAH), indicating a new form of the S1R2 diastereomer.

Other grinding experiments involved a racemic mixture of at least one of the components (RS1 + S2, S1 + RS2, and RS1 + RS2). These also show patterns different from the reactants, but interestingly, the combinations RS1 + S2 and RS1 + RS2 show a pattern similar to that of diastereomer S1R2. On the other hand, S1 + RS2 shows a pattern similar to the other diastereomer S1S2. However, some small variations can be noted when carefully examining these patterns. Some peak positions are slightly shifted in both directions, as shown in Figure S2. Such an observation is indicative of small lattice changes, and hence of solid solution formation. Due to the lack of homogeneity inherent to grinding experiments, and the remaining presence of traces of starting materials, this feature was further investigated using solution-based crystallization experiments. To prove the existence of solid solutions for both diastereomers S1S2 and S1R2 evaporative crystallizations of the combinations S1 + R2, RS1 + R2, S1 + RS2, and RS1 + RS2 in various solvents were analyzed by SC-XRD.

All structures obtained show equimolar amounts of **1** and **2** and crystallize in the monoclinic space group $P2_1$. The structure of S1R2 confirms a new polymorph of the previously reported cocrystal. Multiple crystallization experiments were performed trying to reproduce the previously published polymorph, but all attempts failed. This pushes us to believe that the polymorph described here is the most stable one, even though this would require further confirmation. The major difference between both polymorphs of S1R2 lies in their packing arrangement. The carboxylic acid-amide synthon formed with the amide of S1 involves a different carboxylic acid group of R2 in the two polymorphs. R2 contains two carboxylic acid groups, one attached to C2 (the chiral center) and the other attached to C3 (the methylene next to the chiral center) as shown in Figure 4. In the previously published polymorph, Form I, the synthon is formed using the carboxylic acid at C1 (Figure 4a). In contrast, the second polymorph found in this article (Form II) is constructed through a

https://doi.org/10.1021/acs.cgd.4c00074
Cryst. Growth Des. 2024, 24, 2977−2984

Table 1. Selected Crystallographic Data for Solid Solutions of Phase A (S1R2, $S1R2_{ss}$ with X_{R1} = 0.28, and R1S1-R2S2), and Phase B (S1S2 and $S1S2_{ss}$ with X_{R2} = 0.08)

	cocrystal[a]	*a* (Å)	*b* (Å)	*c* (Å)	space group	*β* (°)	*V* (Å^3)	*ρ* (g/cm^3)
phase A	S1R2 (pure)	11.0560(10)[b]	15.3096(18)	9.4335(10)[b]	$P2_1$	98.730(9)	1578.2(3)	1.272
	$S1R2_{ss}$ (X_{R1} = 0.28)	11.1547(10)[b]	15.3203(14)	9.3593(11)[b]	$P2_1$	99.632(10)	1576.9(3)	1.273
	R1S1-R2S2 (racemic)	11.1180(5)	15.4837(6)	9.1891(6)	$P2_1/c$	98.959(5)	1562.59(13)	1.285
phase B	S1S2 (pure)	12.0408(8)	5.9067(3)	12.1169(8)	$P2_1$	113.961(8)	787.51(9)	1.275
	$S1S2_{ss}$ (X_{R2} = 0.08)	12.095(2)	5.8773(9)	12.153(3)	$P2_1$	114.10(2)	788.6(3)	1.273

[a]The starting compositions in crystallizations of each cocrystal are shown in Table S1. [b]*a* and *c*-axis are swapped for ease of comparison.

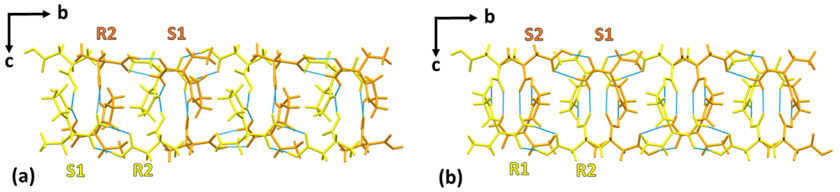


Figure 6. Comparison of crystal packing along *b*-axis of (a) S1R2 Form II and (b) R1S1-R2S2.

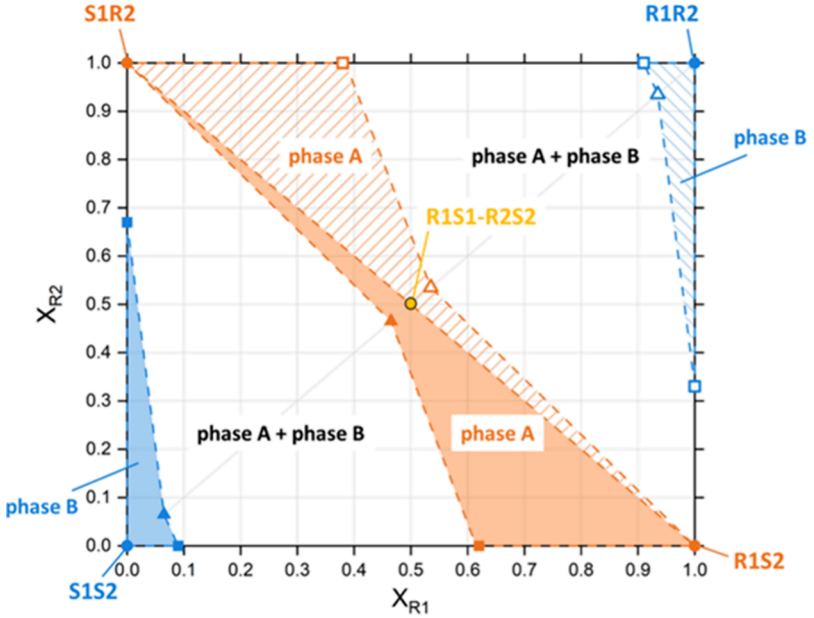


Figure 7. Solid-state stability diagram of **1** and **2**. In the diagram: filled symbols are the composition calculated from the crystal structure, hollow symbols are the mirror points of the filled symbols, square symbols are the miscibility limits obtained from SC-XRD data, and triangular symbols are the median of the limit range obtained from grinding results.

synthon with the other carboxylic acid group at C4 (Figure 4b).

The asymmetric unit of Form II contains two configurations of S1--R2 pairs in which each is connected by a carboxylic acid-amide synthon. These two S1--R2 configurations lead to two different spirals along the *b*-axis which are stacked repetitively along the *a*-direction through hydrogen bonds, as shown in Figure 5a,b. The *ab* plane layers are formed from stacking these spirals which are connected through hydrophobic interactions along the *c*-axis (Figure 5b). Figure S5 shows that the simulated pattern of Form II matches the LAG experimental data. This phase (S1R2) will be called phase A and the combination S1S2 (CSD-REFCODE ROQLEQ) will be called phase B throughout the remainder of the study.

Crystallization of RS1 + RS2 combination resulted in cocrystal R1S1-R2S2. Interestingly, the solid cocrystal phase between both racemates R1S1-R2S2 shows a pattern matching that of phase A. As there is no disorder in this specific case, the R1S1-R2S2 cocrystal is structurally equivalent to that of S1R2 (Table 1). Comparing cocrystals R1S1-R2S2 and S1R2, a difference is observed in enantiomeric configuration. S1 in the yellow spiral of S1R2 (Figure 6a) is replaced by R1 in R1S1-R2S2 (Figure 6b) and, on the contrary, R2 in the orange spiral of S1R2 (Figure 6a) is substituted by S2 (Figure 6b). Therefore, the packing of R1S1-R2S2 is formed by repeated stacking of spirals between R1--R2 (yellow) and S1--S2 (orange) pairs.

Evaporative crystallization of mixtures of RS1 + R2 and S1 + RS2, led to phases A and B, respectively. Single crystals taken from the first combination show a solid solution of phase A (corresponding to the structure of S1R2 with S1 being substituted by R1 with a mole fraction of 0.28 ($S1R2_{ss}$, X_{R1} = 0.28)), while single crystals from the second combination are a solid solution of phase B (S1S2 with S2 being substituted by

https://doi.org/10.1021/acs.cgd.4c00074
Cryst. Growth Des. 2024, 24, 2977−2984

R2 with a mole fraction of 0.08 ($S1S2_{ss}$, X_{R2} = 0.08)). The solid solution in both phases appears as R/S-disorder of compounds **1** and **2** respectively (Figures S3 and S4). The disorder only causes slight changes of the unit cell dimension compared to those of pure phases S1R2 and S1S2 respectively (Table 1). Figures S5 and S6 shows a comparison between the simulated patterns of these solid solutions and confirms the small peak shifts in XRPD observed in the exploratory grinding experiments are indeed due to solid solution formation.

These results indicate that solid solutions occur for both phases A and B. Going from S1-R2 to S1-S2 (or from S1-R2 to R1-R2) (see Figure 7), a phase change occurs from phase A to phase B with both phases corresponding to partial solid solutions. The partial solid solution of phase A corresponds to the structure of S1R2 in which R2 can be partially replaced by S2, or S1 partially by R1. The partial solid solution of phase B corresponds to the structure of S1S2 in which S2 can be partially replaced by R2, or S1 by R1. As the examples of solid solution in Table 1 are obtained from zones (see Table S1) where only one partial solid solution crystallizes, they do not represent the miscibility limits of the solid solution.

To determine the miscibility limits of both solid solutions, a full solid-state stability diagram was constructed (Figure 7) as a square diagram for which each point shows the thermodynamic solid outcome of an equimolar mixture of **1** and **2**, but varying enantiomeric composition of both. Corners represent a cocrystal pair between enantiopure compounds of **1** and **2**. Lateral sides of the diagram link diastereomeric cocrystals, whereas the diagonals connect true isomers. Diagonals divide the diagram into two symmetry related counterparts.

Initial estimation of the miscibility limits (Figure S7) is done through LAG experiments (Figures S8−S10). The phase identification was executed based on the appearance of the characteristic peaks of phase A and B which were assigned at 2θ = 9.9, 11.6, 16.3, and 19.9° for phase A and 2θ = 13.5 and 17.3° for phase B. Starting at the bottom left corner (S1S2−phase B), the vertical axis is identified by varying the *ee* of compound **2** going from enantiopure S2 (X_{R2} = 0) to enantiopure R2 (X_{R2} = 1). Only phase B is observed for $X_{R2} \leq$ 0.60. For X_{R2} = 0.75 and 0.90, a mixture of phases A and B is observed highlighted by the appearance of characteristic diffraction peaks of phase A. Based on these findings, the miscibility limit of R2 in phase B lies somewhere between X_{R2} = 0.60 and X_{R2} = 0.75, and the miscibility limit of S2 in phase A between X_{R2} = 0.90 and X_{R2} = 1.00 (X_{S2} = 0.00−0.10). Starting once more in the bottom left corner, but this time looking at the horizontal axis (varying the *ee* of compound **1** going from enantiopure S1 (X_{R1} = 0) to enantiopure R1 (X_{R1} = 1)), phase B is detected at $X_{R1} \leq$ 0.10 and phase A is detected at $X_{R1} \geq$ 0.75. For X_{R1} = 0.25 and X_{R1} = 0.50 both phases are detected. Therefore, the miscibility limit of R1 in phase B is between X_{R1} = 0.10 and X_{R1} = 0.25 and of S1 in phase A between X_{R1} = 0.50 and X_{R1} = 0.75. The summarized results are shown in Table S2.

Toluene cooling crystallization experiments were performed, and the outcome was examined to pinpoint the exact miscibility limits. To do so, single crystals were analyzed from an experiment in which both phases A and B crystallized.[a] Crystallization conditions were selected based on the LAG results shown in Figure S7. The selected compositions are at coordinates (0.00,0.80) and (0.40,0.00) which are within two phase zones. After cooling, suitable crystals were analyzed by SC-XRD. The crystallization experiment starting from an overall composition (0.00,0.80) produced crystals of phases A and B with composition calculated from SC-XRD of (0.00,1.00) and (0.00,0.67) respectively. Phase A is pure cocrystal S1R2 with no substitution of R2 by the counter enantiomer S2. Either there is no disorder, or the disorder is very small (X_{S2} < 0.05). For cocrystal S1S2 (Phase B), S2 can be freely substituted with R2 up to X_{R2} = 0.67. The crystallization experiment performed at composition of (0.40,0.00) led to phases A and B of respectively (0.62,0.00) and (0.09,0.00). Based on symmetry in the diagram, this implies that starting from the cocrystal S1R2 (phase A), S1 can be freely substituted with R1 up to X_{R1} = 0.38. Alternatively, starting from S1S2 (phase B) S1 can be freely substituted with R1 up to X_{R1} = 0.09.

At the center of the solid phase diagram (Figure 7), one finds the R1S1-R2S2 cocrystal. As this cocrystal is structurally similar to S1R2, a full solid solution is obtained going from S1R2 to R1S2 (replacing simultaneously S1 with R1 and R2 with S2). For the other diagonal line, going from S1S2 to R1R2, grinding experiments started from S1S2 (bottom left corner) and moved up the diagonal by adding equimolar amounts of R1 and R2. At X_{R1} = X_{R2} = 0.05, only phase B is visible in the powder pattern. Phase A appears at X_{R1} = X_{R2} = 0.08. The two phases remain present up to X_{R1} = X_{R2} = 0.45. At X_{R1} = X_{R2} = 0.48, peaks of phase B are no longer detected−leaving only phase A. Therefore, the limit of phase A is between X_{R1} = X_{R2} = 0.45 and X_{R1} = X_{R2} = 0.48 and of phase B between X_{R1} = X_{R2} = 0.05 and X_{R1} = X_{R2} = 0.08. These limits are indicative (obtained from LAG experiments) and not confirmed by SC-XRD, due to the difficulty in obtaining single crystals. As phases present in less than 5% are typically not detectable, these limits should be taken keeping this error in mind.

Figure 7 shows the complete diagram visualizing the various stability regions of each solid solution. Experimentally determined limits are shown by full symbols, whereas hollow symbols represent the mirrored positions. Dashed lines are built as visual guides, and assumed to be approximate boundary regions between the zones where only a single phase is obtained and the zone where both partial solid solutions are obtained. The solid-phase diagram confirms that both phases A and B form double-sided solid solutions as enantiomers of **1** and **2** can be substituted by either or both of their counter enantiomers, albeit in different fractions. To the best of our knowledge this is the first report of such a complex case, where solid solutions can be formed by changing the enantiomeric excess of either one or both of the composing compounds. Phase A shows a larger single-phase region compared to that of phase B due to the full solid solution along the S1R2 − R1S1R2S2 − R1S2 axis. Starting with S1R2 (phase A), S1 can be substituted up to 0.38 mole fraction with R1 keeping **2** enantiopure. Keeping S1 enantiopure, no substitution of enantiomer **2** seems possible starting from the same point. Starting from S1S2 (phase B), S2 can be substituted by R2 up to 67%. Whereas starting from the same point, keeping S2 enantiopure, S1 can be substituted by R1 by about 9%. Interestingly, simultaneous replacement of both enantiomers of **1** and **2** can occur. Once more starting from S1R2, this can occur all long the S1R2-R1S2 diagonal, with a rather narrow zone around the fully racemic mixture (R1S1-R2S2). Simultaneous replacement along the R1R2-S1S2 axis is rather limited. Based on our diagram, phase A,

https://doi.org/10.1021/acs.cgd.4c00074
Cryst. Growth Des. 2024, 24, 2977−2984

overall, allows for more freedom in adapting enantiomeric ratios.

4. CONCLUSIONS

Combining two chiral compounds, we here highlight the possibility to form solid solutions varying the enantiomeric excess of either or both of the compounds involved. Combining etiracetam (**1**) and methylsuccinic acid (**2**), we show the existence of two diastereomers S1S2 and S1R2 both of which form partial solid solutions due to component disorder. The extent to which the partial solid solution can form for both phases is shown in a solid-state stability diagram. Double-sided solid solutions are obtained, where the replacement of the enantiomers by their counterparts occurs in either one or both components. For phase B (S1S2 or R1R2), up to 67% of the enantiomer of **2** can be replaced by the counter-enantiomer. For phase A (S1R2 or R1S2), up to 38% of the enantiomer of **1** can be replaced by its counterpart. Interestingly, a full solid solution is obtained substituting both components simultaneously along the S1R2−R1S2 axis. This is the first investigation into such a complex system where a solid solution cocrystal allows forming solid phases containing scalemic mixtures of two chiral compounds. These systems offer supplementary degrees of freedom, and hence can in the future be used to further fine-tune physicochemical properties of the resulting phases.

■ ASSOCIATED CONTENT

Supporting Information

The Supporting Information is available free of charge at https://pubs.acs.org/doi/10.1021/acs.cgd.4c00074.

Additional XRPD patterns, crystal structure figures, and crystallization details (PDF)

Accession Codes

CCDC 2326228−2326234 contain the supplementary crystallographic data for this paper. These data can be obtained free of charge via www.ccdc.cam.ac.uk/data_request/cif, or by emailing data_request@ccdc.cam.ac.uk, or by contacting The Cambridge Crystallographic Data Centre, 12 Union Road, Cambridge CB2 1EZ, UK; fax: +44 1223 336033.

■ AUTHOR INFORMATION

Corresponding Authors

Adrian E. Flood − *School of Energy Science and Engineering, VISTEC, Rayong 21210, Thailand;* orcid.org/0000-0003-1691-3085; Email: adrian.flood@vistec.ac.th

Tom Leyssens − *Institute of Condensed Matter and Nanosciences, Université catholique de Louvain, Louvain-La-Neuve 1048, Belgium;* orcid.org/0000-0001-7916-1373; Email: tom.leyssens@uclouvain.be

Authors

Sarita Songsermsawad − *School of Energy Science and Engineering, VISTEC, Rayong 21210, Thailand; Institute of Condensed Matter and Nanosciences, Université catholique de Louvain, Louvain-La-Neuve 1048, Belgium*

Oleksii Shemchuk − *Institute of Condensed Matter and Nanosciences, Université catholique de Louvain, Louvain-La-Neuve 1048, Belgium;* orcid.org/0000-0003-3003-3922

Koen Robeyns − *Institute of Condensed Matter and Nanosciences, Université catholique de Louvain, Louvain-La-Neuve 1048, Belgium;* orcid.org/0000-0002-4763-4217

Fuli Zhou − *Institute of Condensed Matter and Nanosciences, Université catholique de Louvain, Louvain-La-Neuve 1048, Belgium*

Complete contact information is available at: https://pubs.acs.org/10.1021/acs.cgd.4c00074

Author Contributions

The manuscript was written through contributions of all authors. All authors have given approval to the final version of the manuscript.

Notes

The authors declare no competing financial interest.

■ ACKNOWLEDGMENTS

The authors would like to thank the FNRS for financial support (PDR T.0262.20).

■ ADDITIONAL NOTE

[a]Limits are based on analysis of one data point. There is a inherent risk of the particle not being at equilibrium due to the incorporation of counter enantiomer in the structure during growth that could be difficult and long. The ee of the particle could therefore be slightly above the true limit of the solid solution.

■ REFERENCES

(1) Kale, D. P.; Zode, S. S.; Bansal, A. K. Challenges in Translational Development of Pharmaceutical Cocrystals. *J. Pharm. Sci.* **2017**, *106* (2), 457−470.

(2) Schultheiss, N.; Newman, A. Pharmaceutical Cocrystals and Their Physicochemical Properties. *Cryst. Growth Des.* **2009**, *9* (6), 2950−2967.

(3) Aitipamula, S.; Banerjee, R.; Bansal, A. K.; Biradha, K.; Cheney, M. L.; Choudhury, A. R.; Desiraju, G. R.; Dikundwar, A. G.; Dubey, R.; Duggirala, N.; et al. Polymorphs, Salts, and Cocrystals: What's in a Name? *Cryst. Growth Des.* **2012**, *12* (5), 2147−2152.

(4) Karimi-Jafari, M.; Padrela, L.; Walker, G. M.; Croker, D. M. Creating Cocrystals: A Review of Pharmaceutical Cocrystal Preparation Routes and Applications. *Cryst. Growth Des.* **2018**, *18* (10), 6370−6387.

(5) Desiraju, G. R. Crystal and co-crystal. *CrystEngComm* **2003**, *5* (82), 466−467.

(6) Aakeröy, C. B.; Salmon, D. J. Building co-crystals with molecular sense and supramolecular sensibility. *CrystEngComm* **2005**, *7* (72), 439−448.

(7) Lusi, M. Engineering Crystal Properties through Solid Solutions. *Cryst. Growth Des.* **2018**, *18* (6), 3704−3712.

(8) Prasad, K. D.; Cherukuvada, S.; Devaraj Stephen, L.; Guru Row, T. N. Effect of inductive effect on the formation of cocrystals and eutectics. *CrystEngComm* **2014**, *16* (42), 9930−9938.

(9) Seera, R.; Cherukuvada, S.; Guru Row, T. N. Evolution of Cocrystals from Solid Solutions in Benzoic Acid−Mono/poly-fluorobenzoic Acid Combinations. *Cryst. Growth Des.* **2021**, *21* (8), 4607−4618.

(10) Cappuccino, C.; Spoletti, E.; Renni, F.; Muntoni, E.; Keiser, J.; Voinovich, D.; Perissutti, B.; Lusi, M. Co-Crystalline Solid Solution Affords a High-Soluble and Fast-Absorbing Form of Praziquantel. *Mol. Pharmaceutics* **2023**, *20* (4), 2009−2016.

(11) Coquerel, G. Review on the heterogeneous equilibria between condensed phases in binary systems of enantiomers. *Enantiomer* **2000**, *5* (5), 481−498.

(12) Barabás, O.; Menyhárd, D. K.; Böcskei, Z.; Simon, K.; Kiss-Ajzert, I.; Takács, K.; Hermecz, I. Structural basis of solid solution formation during chiral resolution. *Tetrahedron: Asymmetry* **2000**, *11* (20), 4061−4070.

(13) Renou, L.; Morelli, T.; Coste, S.; Petit, M.-N.; Berton, B.; Malandain, J.-J.; Coquerel, G. Chiral Discrimination at the Solid State of Methyl 2-(Diphenylmethylsulfinyl)acetate. *Cryst. Growth Des.* **2007**, *7* (9), 1599−1607.
(14) Harmsen, B.; Leyssens, T. Dual-Drug Chiral Resolution: Enantiospecific Cocrystallization of (S)-Ibuprofen Using Levetiracetam. *Cryst. Growth Des.* **2018**, *18* (1), 441−448.
(15) Marc, L.; Lopes, C.; Schneider, J.-M.; Sanselme, M.; Coquerel, G. Impact of a Partial Solid Solution and Water Molecules on the Formation of Fibrous Crystals and Fluid Inclusions. *Crystals* **2021**, *11* (10), 1188.
(16) Chen, S.; Xi, H.; Henry, R. F.; Marsden, I.; Zhang, G. G. Z. Chiral co-crystal solid solution: structures, melting point phase diagram, and chiral enrichment of (ibuprofen)2(4,4-dipyridyl). *CrystEngComm* **2010**, *12* (5), 1485−1493.
(17) Czapik, A.; Jelecki, M.; Kwit, M. Chiral Cocrystal Solid Solutions, Molecular Complexes, and Salts of N-Triphenylacetyl-l-Tyrosine and Diamines. *Int. J. Mol. Sci.* **2019**, *20* (20), 5004.
(18) Scowen, I. J.; Alomar, T. S.; Munshi, T.; Seaton, C. C. Structural similarity in chiral-achiral multi-component crystals. *CrystEngComm* **2020**, *22* (43), 7334−7340.
(19) Sun, J.; Wang, Y.; Tang, W.; Gong, J. Enantioselectivity of chiral dihydromyricetin in multicomponent solid solutions regulated by subtle structural mutation. *IUCrJ.* **2023**, *10* (2), 164−176.
(20) Putman, J. I.; Armstrong, D. W. Recent advances in the field of chiral crystallization. *Chirality* **2022**, *34* (10), 1338−1354.
(21) Calcaterra, A.; D'Acquarica, I. The market of chiral drugs: Chiral switches versus de novo enantiomerically pure compounds. *J. Pharm. Biomed. Anal.* **2018**, *147*, 323−340.
(22) Berry, D. J.; Seaton, C. C.; Clegg, W.; Harrington, R. W.; Coles, S. J.; Horton, P. N.; Hursthouse, M. B.; Storey, R.; Jones, W.; Friščić, T.; et al. Applying Hot-Stage Microscopy to Co-Crystal Screening: A Study of Nicotinamide with Seven Active Pharmaceutical Ingredients. *Cryst. Growth Des.* **2008**, *8* (5), 1697−1712.
(23) Neurohr, C.; Marchivie, M.; Lecomte, S.; Cartigny, Y.; Couvrat, N.; Sanselme, M.; Subra-Paternault, P. Naproxen−Nicotinamide Cocrystals: Racemic and Conglomerate Structures Generated by CO2 Antisolvent Crystallization. *Cryst. Growth Des.* **2015**, *15* (9), 4616−4626.
(24) Harfouche, L. C.; Couvrat, N.; Sanselme, M.; Brandel, C.; Cartigny, Y.; Petit, S.; Coquerel, G. Discovery of New Proxyphylline-Based Chiral Cocrystals: Solid State Landscape and Dehydration Mechanism. *Cryst. Growth Des.* **2020**, *20* (6), 3842−3850.
(25) Buol, X.; Caro Garrido, C.; Robeyns, K.; Tumanov, N.; Collard, L.; Wouters, J.; Leyssens, T. Chiral Resolution of Mandelic Acid through Preferential Cocrystallization with Nefiracetam. *Cryst. Growth Des.* **2020**, *20* (12), 7979−7988.
(26) Rapeenun, P.; Gerard, C. J. J.; Pinètre, C.; Cartigny, Y.; Tinnemans, P.; de Gelder, R.; Flood, A. E.; ter Horst, J. H. Searching for Conglomerate Cocrystals of the Racemic Compound Praziquantel. *Cryst. Growth Des.* **2024**, *24* (1), 480−490.
(27) Teng, Y.; Gu, C.; Chen, Z.; Jiang, H.; Xiong, Y.; Liu, D.; Xiao, D. Advances and applications of chiral resolution in pharmaceutical field. *Chirality* **2022**, *34* (8), 1094−1119.
(28) Eddleston, M. D.; Arhangelskis, M.; Friščić, T.; Jones, W. Solid state grinding as a tool to aid enantiomeric resolution by cocrystallisation. *ChemComm* **2012**, *48* (92), 11340−11342.
(29) Springuel, G.; Leyssens, T. Innovative Chiral Resolution Using Enantiospecific Co-Crystallization in Solution. *Cryst. Growth Des.* **2012**, *12* (7), 3374−3378.
(30) Springuel, G.; Robeyns, K.; Norberg, B.; Wouters, J.; Leyssens, T. Cocrystal Formation between Chiral Compounds: How Cocrystals Differ from Salts. *Cryst. Growth Des.* **2014**, *14* (8), 3996−4004.
(31) Zhou, F.; Shemchuk, O.; Charpentier, M. D.; Matheys, C.; Collard, L.; ter Horst, J. H.; Leyssens, T. Simultaneous Chiral Resolution of Two Racemic Compounds by Preferential Cocrystallization. *Angew. Chem., Int. Ed.* **2021**, *60* (37), 20264−20268.
(32) Zhou, F.; Body, C.; Robeyns, K.; Leyssens, T.; Shemchuk, O. On the pairwise cocrystallization of racemic compounds. *CrystEngComm* **2023**, *25* (20), 3060−3065.
(33) Zeitman, B.; Lawless, J. G. The optical nature of methylsuccinic acid in human urine. *Biochem. Med.* **1975**, *13* (2), 111−116.
(34) Johannessen, S. I. Chapter 9 - Therapeutic drug monitoring of antiepileptic drugs. In *Handb. Anal. Sep.*, Hempel, G., Ed.; Vol. *5*; Elsevier Science B.V., 2004; pp 221−253.
(35) Vardanyan, R.; Hruby, V. Chapter 9 - Antiepileptic Drugs. In *Synthesis of Best-Seller Drugs*, Vardanyan, R., Hruby, V., Eds.; Academic Press, 2016; pp 155−177.
(36) Patsalos, P. N. Pharmacokinetic profile of levetiracetam: toward ideal characteristics. *Pharmacol. Ther.* **2000**, *85* (2), 77−85.
(37) Wang, J.; Yang, Y.; Zhang, R.; Shen, X.; Chen, Z.; Wang, J.; Yuan, Q.; Yan, Y. Microbial production of branched-chain dicarboxylate 2-methylsuccinic acid via enoate reductase-mediated bioreduction. *Metab. Eng.* **2018**, *45*, 1−10.
(38) Rigaku Oxford Diffraction. *CrysalisPro* Software System, Version 1.171.38.41l.; Rigaku Oxford Diffraction Ltd.: Oxford, UK, 2015.
(39) Sheldrick, G. SHELXT - Integrated space-group and crystal-structure determination. *Acta Cryst. A* **2015**, *71* (1), 3−8.
(40) Sheldrick, G. Crystal structure refinement with SHELXL. *Acta Cryst. C* **2015**, *71* (1), 3−8.
(41) Marchand, P.; Lefèbvre, L. c.; Querniard, F.; Cardinaël, P.; Perez, G.; Counioux, J.-J.; Coquerel, G. Diastereomeric resolution rationalized by phase diagrams under the actual conditions of the experimental process. *Tetrahedron: Asymmetry* **2004**, *15* (16), 2455−2465.
(42) McCague, R. A measure of the solid-solution extent useful for crystallisation resolution studies. *Tetrahedron Lett.* **2007**, *48* (5), 869−872.
(43) Tumanova, N.; Tumanov, N.; Robeyns, K.; Fischer, F.; Fusaro, L.; Morelle, F.; Ban, V.; Hautier, G.; Filinchuk, Y.; Wouters, J.; et al. Opening Pandora's Box: Chirality, Polymorphism, and Stoichiometric Diversity in Flurbiprofen/Proline Cocrystals. *Cryst. Growth Des.* **2018**, *18* (2), 954−961.
(44) Tumanova, N.; Tumanov, N.; Fischer, F.; Morelle, F.; Ban, V.; Robeyns, K.; Filinchuk, Y.; Wouters, J.; Emmerling, F.; Leyssens, T. Exploring polymorphism and stoichiometric diversity in naproxen/proline cocrystals. *CrystEngComm* **2018**, *20* (45), 7308−7321.

https://doi.org/10.1021/acs.cgd.4c00074
Cryst. Growth Des. 2024, 24, 2977−2984